International Journal of
Intelligent Systems and Applications in Engineering

ISSN:2147-6799 www.ijisae.org Original Research Paper

Atmospheric and light-induced effects in nanostructured silicon deposited by capacitively and inductively-coupled plasma

Z. M. Saleh[1,3,*], G. Nogay[2,3], E. Ozkol[3], and R. Turan[2,3]

Accepted 15th August 2014 **DOI: 10.18201/ijisae.13913**

Abstract—Renewable sources of energy have demonstrated the potential to replace much of the conventional sources but the cost continues to pose a challenge. Efforts to reduce cost involve highly efficient and less expensive materials as well as enhanced light management. Nanostructured materials consisting of silicon quantum dots in a matrix of amorphous silicon (a-Si) are promising for higher efficiency and better stability. Quantum confinement offers a tunable band gap, relaxes momentum conservation rule, and may permit multi exciton generation, MEG. We employ electron spin resonance (ESR), the temperature dependence of dark and photoconductivity to compare the stability of amorphous and nanostructured silicon films deposited by inductively- and capacitively-coupled plasma against atmospheric and light exposure. Distinctly different behaviors are observed for amorphous and nanostructured films suggesting that nanostructured films are more permeable to oxygen infusion but more resistant to light induced effect.

Keywords—Photoconductivity, amorphous, nanostructure, atmospheric aging, electron spin resonance.

1. Introduction

Global energy consumption is expected to increase significantly over the coming decades. Renewable sources of energy have demonstrated the potential to replace much of the conventional sources but the cost continues to pose a major challenge. Experts estimate that a cost differential of over ten times will continue for the next few decades. Naturally, research and development are focused on improving conversion efficiency as well as reducing cost.

Efforts to reduce cost focus on less expensive and more efficient materials for the solar cell absorber layer, improved solar cell design and better light trapping schemes for higher absorption of incident solar light. All three approaches target the production of efficient devices at low cost. Crystalline silicon is the most widely material to produce devices with fairly high efficiency but it is costly to produce. Amorphous silicon is produced at a fairly low cost but suffers from low efficiency, light-induced metastability [1], [2].

Nanostructured materials in the form of quantum dots in a matrix of a-Si or SiO2 combine the higher mobility and stability of crystalline silicon and the low cost of amorphous silicon [3], [4]. Furthermore, the quantum confinement associated with the quantum dots offers a tunable band gap enabling the production of cells in tandem, relaxes momentum conservation rule allowing transitions in indirect bandgap materials, and may permit the generation of more than one exciton per high-energy photon [5], [6], [7].

Processing of nanostructured silicon employs the conventional capacitively-coupled plasma enhanced chemical vapour deposition (CC-PECVD) with heavy hydrogen dilution of silane. This process produces good quality films but needs large amounts of hydrogen and suffers from low deposition rates both of which add to the cost. Recent attention has been made to inductively-coupled plasma where the nanostructured phase is achieved by increasing RF power with minimal additional cost.

Recent studies suggest that nanostructured materials are more resistive to light-induced degradation (LID) and correlate that effect to the volume fraction of the amorphous component [8], [9]. Due to the long measurements of (LID), these studies are never conclusive.

Nanostructured materials may be less compact and allow oxygen infusion or adsorption with dramatic effects on the optoelectronic properties [8]. Finger et al conducted a thorough investigation of atmospheric aging on samples with various microcrystalline contents and conclude that the dark conductivity (σ_D) may increase or decrease with aging in de-ionized water (DIW) or pure oxygen at 80 ^oC depending on sample structure and history [10]. Some of these defects are irreversible under normal annealing conditions [10], [11], [12].

In this work, we use electron spin resonance, temperature dependence of dark and photoconductivity to examine the stability of amorphous (a-Si:H) and nanostructured (nc-Si:H) silicon, deposited by the capacitively and inductively-coupled plasma enhanced chemical vapour deposition, against the effects of controlled light and atmospheric exposures.

2. SAMPLES AND EXPERIMENT

A set of nanostructured silicon samples with a varying degree of crystallinity (Xc) are deposited in a capacitively-coupled plasma (CCP), and inductively-coupled plasma (ICP) using the plasma enhanced chemical vapour deposition (PECVD). The nanostructured phase was achieved by heavy hydrogen dilution of silane (SiH4) during deposition for the CCP films and by increasing RF power for the ICP films. The crystalline fraction is estimated by decomposing the Raman spectra [11]. For thin film conductivity samples, aging was performed in pure oxygen chamber at 80 ^oC for up to 30 hours. Identical depositions made on larger substrates were peeled off and collected in quartz tubes for

* Corresponding author: zaki.saleh@aauj.edu
Zaki M. Saleh: Arab American University-Jenin (AAUJ)
Note: This paper has been presented at the International Conference on Advanced Technology&Sciences (ICAT'14) held in Antalya (Turkey), August 12-15, 2014

stronger ESR signals. These samples were aged in deionized water (DIW) at 80 ºC which has been reported to be equivalent to the pure oxygen treatment. Light induced degradation was evaluated by exposing the samples to a collimated light equivalent to 10 suns from a halogen lamp. Temperature dependent measurements were obtained by measuring the dark conductivity ($\sigma_{D)}$ using a hotplate equipped with N2 flow to retard atmospheric agents. Thermal activation is performed by measuring σ_D during heat-up form room temperature to 190 ºC, while thermal relaxation is performed during the cool down after a 30-min anneal at 190 ºC. Photoconductivity is measured in situ by illuminating the sample with a red light from a He-Ne laser using standard coplanar geometry with a two rectangular electrodes separated by a 0.5 mm gap [7].

TABLE-1: Nanostrucutred samples used in this study where the ratio of silane to hydrogen ratio is decreased from 10 % (amorphous) to 1 % highly nanocrystalline (Xc ~ 67 %).

Run	SiH_4/H_2 (sccm)	Add H_2 (sccm)	RF Power (Watt)	$SiH_4/(SiH_4+H_2)$
C-10	250	0	50	10
C-12	125	375	50	2.5
C-15	55	495	300	1.0
I-18	90	0	1000	10
I-19	45	180	3000	2.0

2. Results

Figure 1 shows the Raman spectra for amorphous (C-10) and nanostructured (C-15) silicon samples. Nanostructured, C-15 consists of a nanocrystalline phase of approximately 60 % as represented by the narrow component of the spectrum [13].

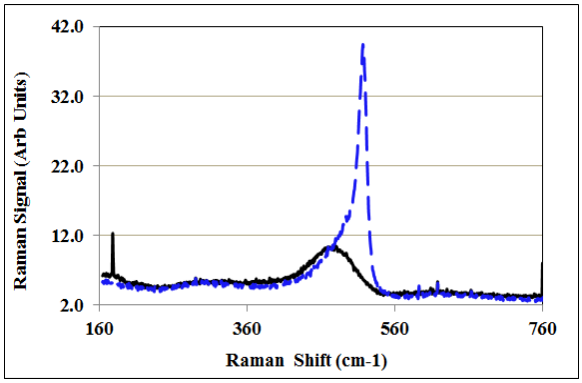

Fig. 1: Raman spectra for amorphous C-10 (solid line) and nanostructured C-15 (dashed line). Coloured online.

To evaluate the stability of these films under prolonged light exposure, we exposed both films simultaneously to a collimated light from a powerful halogen lamp with intensity equivalent to 10 suns. The photoconductivity (σ_{ph}) and dark conductivity (σ_D) were measured in-situ with and without light from a He-Ne laser (λ = 633 nm, I = 3 mW/cm^2), respectively. As shown in Fig. 2, the dark conductivity of a-Si falls below the detection limit of our measurements so any expected change with light exposure is not detectible. The photoconductivity, on the other hand, is a few orders of magnitude higher and its degradation with light exposure is very clear. For nc-Si:H, both dark- and photoconductivity are above our detection limit even at room temperature but still no appreciable degradation is detected in either one for up to 100 minutes of light exposure.

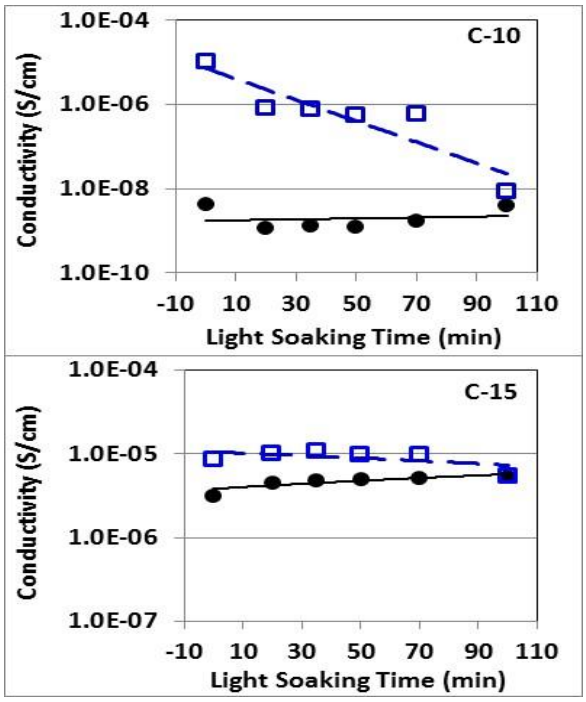

Fig. 2: Dark (solid symbols) and photoconductivity (open symbols) versus light exposure time from a halogen lamp of 10 suns for: (a) a-Si sample (S0) and (b) nc-Si sample (S2).

Figure 3 shows the thermal activation curves, represented by dark

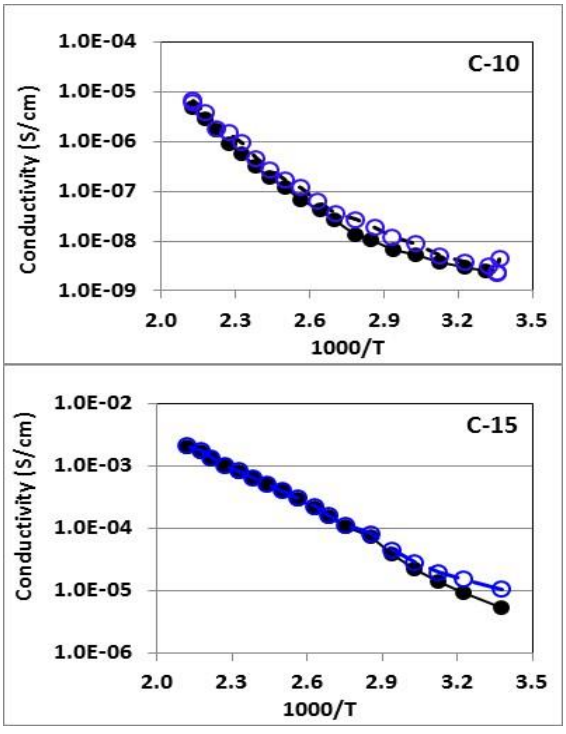

Fig. 3: Activation and relaxation curves for a-Si (C-10) and nc-Si (C-15) in the as-aged state. Solid symbols represent the activation curves from room temperature to 190 C, while open symbols represent the relaxation to room temperature after a 30-min anneal at 190 C. Coloured online.

conductivity versus inverse temperature, for a-Si:H (C-10) and nc-Si:H (C-15) during heating (solid symbols) and cooling after a 30 min anneal at 190 ºC (open symbols). The curves for a-Si (C-10) do not fit a straight line indicating that more than one activation mechanism may be involved.

The curves for C-15, appear to fit a straight line fairly well and single activation energies may be defined. It is also noticed that the cooling curve (open symbols) for C-10 differs from the heating curves only slightly, while that for C-15 begins to depart from the heating curve as the sample approaches room temperature.

In Fig. 4, we present the activation and relaxation data for the same two samples (C-10 and C-15) after an exposure of 30 hours to pure oxygen at 80 C. The activation curve for C-10 are pretty similar to those obtained before oxygen exposure (Fig. 3) while those for C-15 depart significantly from the straight line behaviour observed before oxygen exposure. Furthermore, the relaxation data remain higher than the activation data although they fall to a similar value at room temperature after a long time.

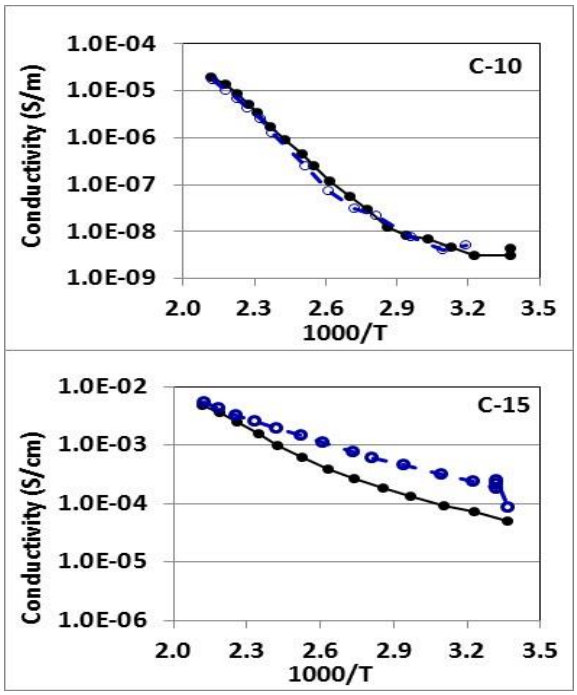

Fig. 4: Activation and relaxation curves for a-Si (C-10) and nc-Si (C-15) in the oxygen exposed state. Solid lines and symbols represent the activation from room temperature to 190 ºC, open symbols represent the relaxation to room temperature after a 30-min anneal at 190 ºC. Coloured online.

In Fig. 5, we compare the activation and relaxation curves for sample I-18 (amorphous) and I-19 (nanostructured) in the as-grown state. The dark conductivity is higher for the nanostructured sample at all temperatures as expected but sample I-19 exhibits distinctly different relaxation behaviour.

Even though the measurements are taken simultaneously for both samples after only two days of storage in desiccator, the relaxation curve for I-18 follows the activation curve fairly well, while that for I-19 departs significantly for T > 240 ºC, although they fall back to similar values at room temperature but only after several hours. This result suggests that a very slow annealing mechanism may be involved. Ironically, this film in its as-grown state behaves somewhat similar to C-15 in its oxygen-exposed state (Fig. 4).

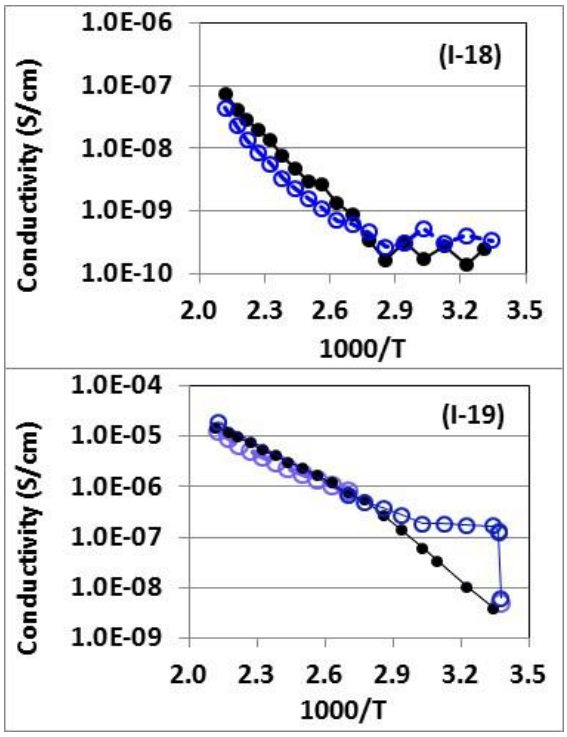

Fig. 5: Activation and relaxation curves for amorphous a-Si (I-18) and nanostrucutred nc-Si:H (I-19) both deposited by ICP-CVD in the as grown-state. Solid symbols represent the activation from to 190 ºC, open symbols represent relaxation to room temperature after a 30-min anneal at 190 C. Coloured online.

In Fig. 6, we show the activation and relaxation curves for both samples in the oxygen-exposed state. No significant changes occur for amorphous sample I-18 while the effect is dramatic for I-19. The relaxation curve for the O2-exposed state of I-19, shows a rather interesting if not bizarre behaviour near room temperature.

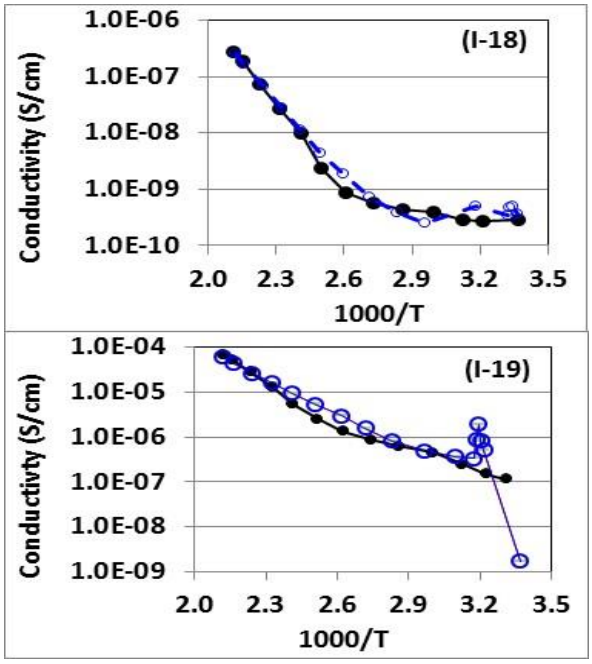

Fig. 6: Activation and relaxation curves for amorphous a-Si (I-18) and nanostrucutred nc-Si:H (I-19) both deposited by inductively coupled plasma CVD in the as oxygen-exposed state. Solid symbols represent the activation from to 190 ºC, open symbols represent relaxation to room temperature after a 30-min anneal at 190 C. Coloured online

To understand the origin of the defects causing these changes in the activation and relaxation behaviours, we compare the electron spin resonance (ESR) spectra for low Xc (C-12) and high-Xc (C-15) powdered samples. Powdered samples for the amorphous (C-10) and both ICP samples (I-18 and I-19) were difficult to obtain due to strong adhesion to the substrates. The ESR signal obtained in the dark is commonly linked to the neutral dangling bond centres (D^o).

As shown in Fig. 7, the ESR signal attributed to Do decreases upon aging in DIW at 80 ^oC for two days for both samples but the decrease for sample (CCP-15) with higher Xc appears to be larger. The larger DIW-induced decrease in ESR for C-15 suggests that the nanostructure phase is more susceptible to oxygen infusion that may alter band gap defects. The decrease in ESR with DIW-soaking is expected to be much less for the amorphous sample (Xc = 0).

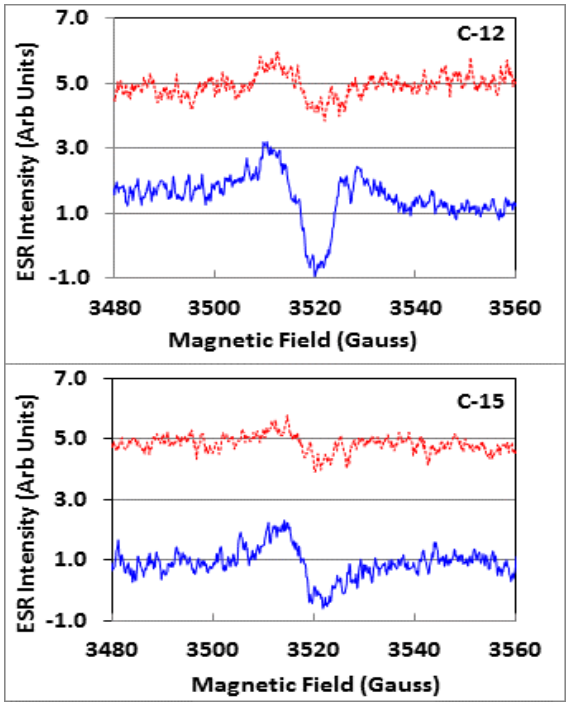

Fig. 7. Dark ESR spectra for C-12 with low Xc content and C-15 with higher Xc content silicon samples in the as-grown (lower solid line) and aged (upper dotted line). Spectra are coloured online.

3. DISCUSSION

Important differences in the annealing, oxygen-exposed and light-exposed behaviours of nanostructured and amorphous silicon are observed by several techniques for both CCP and ICP films. The dark conductivity for nc-Si:H is several orders of magnitude higher than that of a-Si:H owing to the higher mobility associated with the nanostructure. While the relaxation curve follows the activation curve for a-Si:H, it stays at higher values for nc-Si:H above 250 ^oC, although it continues to relax at room temperature for several hours. We attribute this behaviour to a very slow annealing process of native or adsorbed defects.

Another difference is that the activation and relaxation curves for a-Si:H are not affected by O2-exposure, but differ significantly for nc-Si:H as indicated in Fig. 3 and Fig. 4. The linear dependence of both curves in the as-aged state bends for nc-Si:H after O2-exposure suggesting that an additional activation mechanism may be introduced by O2-exposure.

The results for the ICP samples (I-18 and I-19) in the as-grown state behave similar to C-15 after oxygen exposure at 80 ^oC. ICP films have been shown to absorb oxygen readily even at room temperature. The absence of stronger effect for I-19 with higher nanocrystalline content may be explained in terms of stronger O_2 infusion leading to saturation before further O_2-exposure at 80 ^oC. Enhanced conductivity suggests that defects acting as recombination centres are being shifted towards the conduction band edge and becoming trap-like defects. Such defect conversion is expected to decrease the dark ESR signal. The similar although not identical treatment caused the ESR signal to decrease for nanostructured silicon and more so for the sample with higher nanocrystalline content (C-15) agrees with this conclusion.

Veprek et al propose a passivation of defects residing at the grain boundaries due to oxygen infusion or adsorption, suggesting that the defect density may actually decrease with O2-exposure [14]. Our ESR results for nc-Si:H agree with this prediction but DBP results conducted earlier on identical samples exhibit no changes in the occupation of defects below the Fermi level due to O2-exposure [7]. The decrease in Do as detected by ESR may actually be related to defect charging.

The decrease in the dark conductivity and the increase in sub-band-gap absorption due to light exposure as was reported earlier is expected for a-Si:H. However, no change in dark- or photoconductivity is observed for nc-Si:H after similar light exposure conditions of over 100 minutes under a light intensity of 10 suns. It is clear that this exposure time even under 10 suns is not sufficient to make satisfactory conclusions and further investigations involving ESR and photoconductivity are clearly needed.

It is interesting to note that the two structural phases of silicon behave in strikingly opposite ways under oxygen and prolonged light exposures. Amorphous silicon properties degrade significantly due to light exposure but they appear resistive to O2-aging, while the properties of nc-Si:H are susceptible to O2 infusion while those of a-Si:H are not.

4. CONCLUSION

We have explored an important approach to enhance the optoelectronic properties of amorphous and nanostructured Si against atmospheric and light exposure for potential use in photovoltaic devices. Distinctly different activation and relaxation behaviours are observed for these structural phases of silicon. The conductivity for nc-Si:H is several orders of magnitude higher than a-Si:H but the photo-response for nc-Si is lower. Nanostructured silicon appears more susceptible to oxygen infusion and the affect is more dramatic for the ICP films. The apparent increase in dark conductivity following oxygen exposure for both nanostructured film and the decrease in dark ESR signals are consistent with the passivation of defects residing at grain boundaries. The different relaxation behaviours for nc-Si:H is attributed to a very slow annealing mechanism.

ACKNOWLEDGEMENT

This study has been supported by the Scientific and Technological Research Council of Turkey (TUBITAK). Zaki M. Saleh acknowledges support from the Scientific and Technological Research council of Turkey (TUBITAK) under grant no (TUBITAK-BIDEB-2221).

References

[1] D.L. Staebler, C.R. Wronsky, Appl. Phys. Lett. 31, 292 (1977).

[2] M. Stutzmann, W. B. Jackson and C. C. Tsai: Phys. Rev. B 32, 23 (1985).

[3] C-H. Lee, A. Sazonov, and A Nathan, Applied Phys. Lett. 86, 222106 (2005).

[4] E.C. Cho, M.A. Green, G. Conibeer, D.Y. Song, Y.H. Cho, G. Scardera, S. J. Huang, S. Park, X.J. Hao, Y.D. Huang, L.V. Dao, Adv. Opt. Electron, 2007, 11 (2007).

[5] C. Delerue, G. Allan, and M. Lannoo, Phys. Rev. B, 48, 11024 (1993).

[6] J. Heitmann, F. Müller, L. X. Yi, M. Zacharias, D. Kovalev, F. Eichhorn, Phys. Rev. B 69, 195309 (2004).

[7] A. Nozik, J. Chem. Phys. Lett. 2008, 457, 3 - 11.

[8] J-H Yoon, P.C. Taylor, C-H Lee, Journal of Non-Crystalline Solids 227-230, 324 (1998).

[9] F. Finger, R. Carius, T. Dylla, S. Klein, S. Okur, M. Günes, Journal of Optoelectronics and Advanced Materials, 7, 83 (2005).

[10] Smirnov, S. Reynolds, F. Finger, R. Carius, C. Main, Journal of Non-Crystalline Solids 352, 1075 (2006).

[11] M. Gunes, H. Cansever, G. Yilmaz, V. Smirnov, F. Finger, R. Brüggemann, Journal of Non-Crystalline Solids, 358, 2074 (2012).

[12] D. Song, E.-C. Cho, G. Conibeer, C. Flynn, Y. Huang, M.A. Green, Solar Energy Materials and Solar Cells 92/4 (2008) 474.

[13] S. Veprek, Z. Iqbal, R.O. Kuhne, P. Capezzuto, F.A. Sarott, and J.K. T. Sako, H. Kiyoto, H. Terauchi, and T. Imura, J. Non-Cryst. Solids 59 & 60, 791 (1983).